

Published in final edited form as:

J Phys Chem A. 2012 May 3; 116(17): 4274–4284. doi:10.1021/jp2108363.

Mechanistic insights into the Structure and Dynamics of Entangled and Hydrated Lambda-Phage DNA

Sandipan Chakraborty^{1,^}, Takashi Uematsu^{2,§,*^}, Christer Svanberg^{2,§}, Per Jacobsson², Jan Swenson², Michael Zäch², Rajendar Trehan³, George Armstrong³, and Bidisha Sengupta^{3,*}

¹Saroj Mohan Institute of Technology, West Bengal, India

²Department of Applied Physics, Chalmers University of Technology, SE-412 96 Göteborg, Sweden

³Department of Chemistry, Tougaloo College, Tougaloo, MS, 39174, USA

Abstract

Intrinsic dynamics of DNA plays crucial role in DNA-protein interactions and has been emphasized as a possible key component for *in vivo* chromatin organization. We have prepared entangled DNA micro tube above the overlap concentration by exploiting the complementary cohesive ends of λ -phage DNA, which is confirmed by atomic force microscopy and agarose gel electrophoresis. Photon correlation spectroscopy further confirmed that the entangled solutions are found to exhibit the classical hydrodynamics of a single chain segment on length scales smaller than the hydrodynamic length scale of single λ -phage DNA molecule. We also observed that in 41.6% (gm water/gm DNA) hydrated state, λ -phage DNA exhibits a dynamic transition temperature (T_{dt}) at 187 K and a crossover temperature (T_c) at 246 K. Computational insight reveals that the observed structure and dynamics of entangled λ -phage DNA are distinctively different from the behavior of the corresponding unentangled DNA with open cohesive ends, which is reminiscent with our experimental observation.

Keywords

λ -phage DNA; DNA micro tube; entanglement; Photon correlation spectroscopy; hydrodynamics; glass transition

INTRODUCTION

Concentrated polymer solutions are important in technological applications from two perspectives: synthetic and bio-polymers. For instance, the concentration of DNA in the nucleus of biological cells is far above the overlap concentration of the corresponding DNA polymer solution and the hindered motion of the DNA molecules due to the entanglements may affect the biological function. In the present communication, we use DNA as a model

*Correspondence to Takashi Uematsu (Telephone: +1-46-30388407, FAX: +1-46-30386649, takashiolga@gmail.com); Bidisha Sengupta (Telephone: +1-601-977-7779, FAX: +1-601-977-7898, bsengupta@tougaloo.edu).

[^]Authors contributed equally to the work.

[§]Present address: Borealis AB, SE-444 86 Stenungsund, Sweden.

SUPPORTING INFORMATION AVAILABLE

Supplemental Figures 1S (A and B) display the importance of segmentation point in determining the stability of the genome while Figure 2S presents the negative correlation of bendability with curvature in the λ -phage genome. This material is available free of charge via the Internet at <http://pubs.acs.org>.

for long polymers to investigate properties of entangled polymers in general, because DNA is an unusually well-characterized bio-polymer regarding molecular structure, dimensions, charge and stiffness.¹ These facts have been exploited in DNA-based studies of the rheological properties of dilute and semi dilute polymer solutions.² The effect of DNA concentrations on the twisting and tumbling of short pieces of DNA has been investigated by steady state fluorescence spectroscopy.³ Although the structure⁴⁻⁷ and global chain dynamics^{8,9} of concentrated DNA-solutions have been investigated in detail, comparatively little is known about the local DNA chain dynamics under such conditions. This served as the motivation to undertake the present study on the effect of increasing concentration on the structure and dynamics of long chromosome-sized DNA. We are particularly interested in differences in bending characteristics of λ -phage DNA upon entanglement due to the fact that bending of duplex DNA has proven to be playing a crucial role in binding with important proteins.^{6,7}

To obtain long DNA polymers we use λ -phage DNA, a double-stranded DNA molecule with a contour length of roughly 16.5 μm .¹⁰⁻¹² Mature λ -phage DNA, as extracted from the phage, is a linear duplex of some 48,500 uniquely ordered base pairs with a 12 nucleotides long protrusion at both the 5'-ends.¹⁰⁻¹² These cohesive ends are complementary to each other. Thus, at room temperature the end-group of one duplex adheres spontaneously to the opposite end of another DNA molecule to form the extended (concatemeric) linear polymer chains.¹³⁻¹⁵ The contour lengths of these DNA micro tubes are counted in multiples of the λ -monomer size which formed the entangled molecules. Importantly, the end-to-end linkages are reversibly broken at 65 °C because the cohesion is based on a limited number of hydrogen bonds.^{14, 15} Even to a lesser extent, circular macromolecules can be formed, with the joining of the end-groups of a single chain¹⁶⁻¹⁹ or those of an extended chain.¹³⁻¹⁵ However, in concentrated solution, spontaneous adhesion of the end-groups of different chains interconnects many λ -phage DNA molecules, resulting in a heavily entangled network, thereby making the solution gel-like.^{14, 15}

The omnipotence of water has exerted a profound influence on the function, specificity and progressive development of DNA stability. Studies on hydrated state are important for better understanding of structure and function of a DNA molecule.²⁰⁻²⁶ The influence of water on the conformation and interactions of nucleic acids has attracted much attention ever since the discovery of the fact that the structure of DNA is related to the relative humidity.²⁰ It is known²¹ that minor groove hydration plays an important role for the structural integrity of duplex DNA. Bound water molecules (corresponding to 30 water molecules per base pair) form a glassy region around DNA and this intervening shell of glassy water links the pure ice and the DNA strands below the glass transition temperature.²⁶⁻²⁸ Nevertheless, much remains to be understood about the structure and dynamics of both hydrated groove and surface region of DNA, their significances and differences. Hence we undertook a preliminary investigation on the dynamics of λ -phage DNA in hydrated state.

Four issues about structure and dynamics of λ -phage DNA in aqueous solution and hydrated state have been addressed in this paper:

1. "How the structure and size-distribution of the entangled λ -phage DNA vary compared to the unentangled one", were investigated using atomic force microscopy (AFM) and agarose gel electrophoresis (AGE), respectively.
2. "To what extent these structural variations alter the dynamics of entangled DNA", were studied by photon correlation spectroscopy (PCS).
3. "What are the different types of bends induced by the entanglement on the λ -phage DNA molecule and the relation of the bends to the local structural variations", were investigated using computational chemistry.

4. “What is the nature of the dynamic behavior of λ -phage DNA in 41.6% (gm water/gm DNA) hydrated state and is this dynamics coupled to its surrounding environment”, was studied by differential scanning calorimetry (DSC).

Entangled λ -DNA solutions were prepared above the overlap concentration, c^* (30–50 $\mu\text{g/ml}$)^{10–12} of λ -phage DNA, and subsequently diluted before the investigations. We demonstrate here that the initially entangled solutions retain an entangled network even when the solutions are diluted below c^* due to the hybridized DNA molecules, in contrast to that of the unentangled DNA solutions obtained with a quenching method.^{10–12,14–17} Furthermore, we show that the hydrodynamic correlation length of the entangled network is less than the hydrodynamic diameter of one λ -phage DNA molecule, reflecting a structural memory of the coil-overlapping conditions during sample preparation.

EXPERIMENTAL

Materials

The λ -phage DNA was received from Sigma-Aldrich in lyophilized (freeze-dried) form. Agarose was obtained as powder from Pronadisa, and low-melt agarose powder was from Biorad. For the size-standards for the gel electrophoresis, a pre-formed λ -ladder in gel plugs (New England Biolabs) was used with a total DNA concentration of 50 $\mu\text{g/ml}$.

Aqueous entangled solutions of λ -phage DNA were prepared by dissolving the lyophilized DNA in TE buffer (10 mM Tris-HCl, 1 mM EDTA) with 100 mM NaCl added, for at least five days at room temperature.^{14–17} In order to facilitate adhesion of the end-groups between different DNA molecules, the concentration (c) was adjusted to be 6000 $\mu\text{g/ml}$, which is more than one hundred times higher than the overlap concentration $c^* \approx 40 \mu\text{g/ml}$.¹¹ The solutions were thereafter diluted with TE buffer to 300 $\mu\text{g/ml}$, 150 $\mu\text{g/ml}$, 140 $\mu\text{g/ml}$ or 20 $\mu\text{g/ml}$. Reference samples of unentangled DNA molecules were obtained by disjoining the cohesive ends through heating the samples at 65 °C for 10 minutes and quenching them in an ice bath (hereafter referred to as “quenched” samples).^{13,18,19} The quenched and unquenched samples of the λ -DNA were repeatedly examined using both AFM and PCS during one month after preparation, as well as by gel electrophoresis.

Photon Correlation Spectroscopic Measurements

For observation of the DNA polymer dynamics, PCS was performed at 25 °C using a frequency doubled Nd-Vanadate laser (Coherent Inc.), operating at 532 nm and a correlator (ALV-5000/FAST), as a function of the scattering wave vector, q . The samples were prepared by adding an unquenched solution at 20 $\mu\text{g/ml}$ or 140 $\mu\text{g/ml}$ or a quenched solution at 20 $\mu\text{g/ml}$ into a cylindrical sample cell. To check whether the investigated DNA solutions did not contain any dust particles that affect the PCS data, a portion of the quenched solution (at 20 $\mu\text{g/ml}$), that is a solution of unentangled and non-overlapping λ -DNA chains, was filtered with 0.65 μm Millipore membrane (Ultrafree-CL) without any external pressure. The PCS data of the filtered solution was found to be identical within errors to that of the unfiltered solution.

Differential Scanning Calorimetric Measurements

Lyophilized λ -phage DNA (lot # 054K9089) was a product of Sigma. The dry DNA from the bottle was used for the experiments as the dehydrated sample. Hydration was done by keeping the dry DNA in a desiccator containing a saturated solution of NaBr to achieve the relative humidity 57%.²⁰ Under this condition, after seven days the DNA was hydrated to a level of 41.6% (weight of water / weight of DNA). We chose to undertake the present preliminary investigation on this hydrated DNA in order to understand dynamics of DNA

and its surrounding solvent, and how they are related to each other. The final hydration level of around 0.4 was appropriate because we wanted to have the amount of non-crystalline water at the highest possible level without forming a lot of bulk ice in order to maximize the dynamics of DNA (which increases with increasing amount of amorphous water). Thus, our aim was to have as high hydration level as possible without forming a large quantity of bulk ice, and to be as close as possible to this goal a relative humidity of 57% was the best choice. Dehydrated and hydrated DNA samples were then used for differential scanning calorimetric (with TA instruments, DSC Q 1000). The behavior of λ -phage DNA with increasing temperature was studied by DSC at the heating/cooling rate of 10 °C/min. All experiments were carried out between -150 °C and 95 °C. Hermetic pans with a sample volume of about 20 μ l were used for all measurements. The reference cell was an empty hermetic pan with which the instrument was previously calibrated. Each set of experiments were repeated three times in order to satisfy the reproducibility of the data. The program Universal analyses 2000 was used to determine the transition temperature in each case.

AFM measurements

The AFM experiments were performed at room temperature using a PicoSPM microscope in conjunction with a multipurpose large-area AFM scanner, both from Agilent Technologies (formerly Molecular Imaging, Inc.). All images were acquired in constant-force contact mode using commercially available tips and cantilevers with spring constants $k \leq 0.03$ N/m (MSCT-AUHW MicroleversTM, Veeco Europe, France). Typical scan rates were 1-2 lines/s. In order to avoid build-up of multi layers of DNA molecules on the AFM substrates, the quenched and unquenched solutions at 20 μ g/ml were diluted to less than 0.1 μ g/ml by adding TE buffer. The DNA molecules were immobilized on 3-aminopropyl-triethoxysilane (APTES; Sigma-Aldrich) modified muscovite mica (Mica New York Cooperation, USA) substrates. While APTES modification of mica is traditionally carried out in vapor phase,²⁹ we used here a solution-based approach as developed by Liu et al.³⁰⁻³¹ Freshly cleaved mica substrates of 15 mm \times 10 mm size were installed in an open AFM liquid cell and exposed to a solution of 0.1% (v/v) APTES in ultrapure, de-ionized water with resistivity > 18 M Ω /cm for 10 minutes and then rinsed with TE buffer. The APTES-modified substrate was exposed to the DNA-solution for 45 minutes, followed by careful rinsing with TE buffer and subsequent drying in air for 60 minutes. Before the liquid cell was mounted into the instrument, fresh TE buffer was slowly added to the liquid cell. All images were thus acquired in TE buffer.

Agarose gel electrophoresis (AGE)

Agarose gel electrophoresis was used to measure the length-distribution of the hybridised λ -phage DNA. As discussed in detail below, the hybridization was performed inside gel plugs in order to avoid artefacts during the electrophoretic analysis that may arise from gel-trapping of entangled DNA molecules. Agarose gel plugs for DNA hybridization³² were formed by mixing equal volumes of a λ -DNA solution quenched at 300 μ g/ml and a 1.5% low-melt agarose solution at 50 °C, all in TE-buffer. The mixture was allowed to solidify into 0.75% gel-plugs inside a 1 ml plastic syringe kept at ice for 1 hour before the gel plugs were ejected manually and stored in TE-buffer at 8 °C. For DNA-hybridisation a gel plug was transferred to TE-buffer at 20 °C, and aliquots in terms of 2 mm gel-slices were cut from the gel plugs at suitable time intervals for up to one week, and the slices were stored at 8 °C until the electrophoretic analysis was performed. Notably, the hybridisation product cannot be diluted inside the gel plugs, so the DNA concentration is fixed at 150 μ g/ml.

The hybridized λ -phage DNA samples, as well as the reference sample quenched in solution at 150 μ g/ml, were analysed in 1% agarose gels by pulsed field gel electrophoresis³³ at 6 V/cm, using a 120° field angle and a pulse duration $T_p = 30$ s. All gel experiments were

performed in TBE buffer (50 mM Tris, 50 mM Boric acid, 1.25 mM EDTA) at 17 °C. Gels were post-stained with ethidium bromide for 1 hour, and the fluorescence intensity was measured with a Fluoromager 595 gel scanner (Molecular Dynamics) using 514 nm excitation and a 610 nm long pass emission filter.

Sequence analysis and calculation of structural parameters

A full-length sequence of Enterobacteria phage lambda complete genome (gi|215104|), with 48,502 nucleotides long genomic sequence, was obtained from NCBI using entrez search facility. A cumulative GC profile was calculated using GC-profile web-server.³⁴ All the structural parameters of the λ -phage genome were calculated using the DNALive web interface.³⁵ Due to the limitation in the online server, analysis was performed on a 29 kb λ -phage genome.

Curvature and bendability calculation

The curvature and bendability of the λ -phage genome were calculated using both the DNALive³⁵ and the bend-it^{36,37} web-server.

Calculation of energetic and dynamics of entanglement

λ -phage DNA has 12 nucleotide long cohesive ends. Structures of free cohesive ends and the entangled regions in A, B and Z DNA form were built from the sequence using HYPERCHEM molecular building interface using nucleotide databases. Structures were solvated in a periodic box containing 980 water molecules. Each structure was then subjected to minimization using AMBER94 force field implemented in HYPERCHEM. The enthalpy of formation of entangled DNA (ΔE) was calculated using the following equation and is shown by the Scheme 1 below.

$$\Delta E = E_{\text{entangled DNA}} - (E_{3' \text{ sticky ends}} + E_{5' \text{ sticky ends}}) \quad (1)$$

Where $E_{\text{entangled DNA}}$, $E_{3' \text{ sticky ends}}$ and $E_{5' \text{ sticky ends}}$ are the minimum energies of the entangled DNA and the free 3' - and 5' -sticky ends respectively. Calculations were performed on cohesive ends only.

Normal-mode calculations of the λ -phage DNA were carried out using the Elnémo online server.³⁸ 3-D structures were built using HYPERCHEM model builder and subsequently minimized in water using AMBER94 force fields.

Given the coordinates of the DNA, Elnémo builds an elastic network model by using a harmonic potential with a single force constant to account for pair-wise interactions within a cut-off distance. The potential used to build the elastic network representation is:³⁸

$$E_{\text{network}} = \frac{1}{2} \sum_{d_{ij}^0 < R_c} C (d_{ij} - d_{ij}^0)^2 \quad (2)$$

where d_{ij} is the distance between the dynamical coordinates of the i^{th} and the j^{th} atom, and d_{ij}^0 is the distance between the same pair, as given in the structure. C is the spring constant of the Hookean potential (assumed to be the same for all interacting pairs) and R_c is an arbitrary cut-off distance beyond which interactions are not taken into account (Elnémo uses a default cut-off of 8 Å). Default values of the amplitude range and the increment were used to calculate the 100 lowest frequency normal modes. The first six trivial normal modes are discarded because they represent only translation and rotational movement of the

biomolecule. So, modes 7-106 have been analyzed further. Later in this communication, mode 7 has been referred as the lowest frequency mode and other modes have been numbered accordingly.

Chromatin dynamics

Chromatin dynamics was performed using DNALive.³⁵ Upon giving a DNA sequence, DNALive produce a rapid representation of chromatin dynamics using mesoscopic Metropolis Monte Carlo algorithm, where the geometry of each base pair is defined by three local rotations (roll, tilt and twist) and translations (slide, shift and rise), and the conformational energy is estimated from the deformation matrix using a harmonic model (represented by equation 3), where the index 'k' stands for one of the M base pair steps and the index 'l' stands for the six unique helical parameters (ζ) for each step. The equilibrium value for one helical parameter in a given base pair step type (ζ_{kl}^0) and the associated deformation constant ($K_{k,l}$) were previously determined from molecular dynamics simulations.³⁵ Once a movement in helical coordinates is accepted by the Metropolis test, the corresponding Cartesian structure of the fiber is generated.

$$E = \sum_{k=1}^M \sum_{l=1}^6 K_{k,l} (\zeta_{kl} - \zeta_{kl}^0)^2 \quad (3)$$

RESULTS AND DISCUSSION

Structure of entangled and unentangled λ -phage DNA

Figure 1 presents the AFM height images of the quenched (A) and unquenched (B) DNA molecules immobilized onto APTES-modified mica sheets. The quenched (Q) DNA molecules are found as evenly distributed, isolated chains. The observed appreciable elongation is probably due to liquid flow, which occurred when the solution was added on the AFM substrate to immobilize DNA molecules on the surface. In fact, this elongation is a strong evidence that the molecules are not entangled. The unquenched (uQ) DNA molecules, on the other hand, are typically found as large clusters consisting of a large number of DNA molecules (Figure 1B shows the vicinity of the edge of the clusters). The typical mesh radius ($\approx 0.1\mu\text{m}$) is less than the radius of gyration, R_g , ($\approx 0.5\mu\text{m}$)¹¹ of a single λ -DNA molecule. Since the concentration used here is far below the overlap concentration c^* ($\approx 40\mu\text{g/ml}$),¹¹ it is clear that the observed networks are not a result of single DNA molecules being coincidentally overlapped but a direct consequence of the molecules in solution being heavily entangled.

Agarose gel electrophoresis (Figure 2) was used to monitor the lengths of the unquenched (uQ) and quenched (Q) λ -DNA. In the gel-image (Figure 2A) the uQ-zone is more extended than the Q-sample, indicating that hybridization results in longer DNA polymers. Absolute sizes were estimated by comparison with a λ -ladder standard (St), which is resolved up to the 12-mer carried out under the present AGE resolution. The uQ- and Q-samples both lack the discrete zones seen with the size standard, an effect which we ascribe to an intentional DNA-overloading on the gel. In order to approach the conditions used to prepare the AFM and PCS samples the uQ-sample was hybridized at a DNA-concentration ($150\mu\text{g/ml}$), which is three times that of the size standard. This higher concentration is expected to lead to overlapping of bands, and the overloading effect will be even more severe for the Q-sample because the same amount of DNA is concentrated into a narrower zone (Figure 2A).

From the intensity profiles (Figure 2B) it is seen that the uQ-zone extends from the λ -monomer to about the decamer (485 kb). Since a higher DNA concentration promotes

hybridization^{8,16} the samples prepared for PCS and AFM at 6000 μ g/ml are expected to contain λ -concatamers at least as long as the 10-mer. The Q-zone is seen to extend up to the λ -dimer, but it should be kept in mind that the mobility in pulsed field electrophoresis decreases with increasing DNA concentration.³⁹ In fact, the Q-sample is at a concentration (150 μ g/ml) where the λ -monomer mobility is about 30% lower compared to a dilute sample (20 μ g/ml).³⁹ The Q-zone position in Figure 2 is thus consistent with that quenching produces only monomeric λ -DNA. This is also supported by the observation that a decreased loading of the Q-sample resulted in a narrower zone which co-migrated with the λ -ladder monomer (Results not shown).

It should be noted that AGE was used to measure the lengths of the hybridized λ -phage DNA, not to study the DNA-networks that arise when such long molecules become entangled (c.f. Figure 1). Indeed, such networks are unlikely to enter the gel because their mesh-sizes (0.1 μ m) are comparable to the radius-of-gyration of DNA circles known to be arrested by impalement on agarose gel fibres.⁴⁰ The in-gel hybridization approach (see Methods) was used to minimize DNA-DNA entanglements, so that the DNA size-distribution could be measured by gel electrophoresis without interference from such gel-trapping.

Dynamics in entangled and unentangled λ -phage DNA solution

The $g_1(q, t)$ functions were obtained using the Siegert relation³²: $g_1(q, t) = [(g_2(q, t) - 1)/\sigma]^{0.5}$, where $g_2(q, t)$ is the intensity autocorrelation function directly obtained from the correlator, and σ the instrumental coherence factor that was set to unity. To ensure the reproducibility of the data, different scattering volumes in the samples have been also detected. The scattering wave vector was determined using $q = (4\pi n/\lambda) \sin(\theta/2)$, where n is the refractive index set to 1.33 (pure water), λ the wave length of the laser (= 532 nm), θ the scattering angle.

Figure 3 shows typical field correlation functions, $g_1(q, t)$,^{41,42} for the quenched and unquenched DNA solutions. The observed relaxation process is normally attributed to the collective dynamics of the polymer network, often observed as a simple exponential decay in synthetic polymer solutions.⁴¹ However, the observed process is a short-time exponential decay that develops to a broad relaxation decay. The whole process is well described by the empirical function:⁴³

$$g_1(q, t) = \frac{A}{\left[1 + \frac{\sqrt{1-a}}{a} \frac{t}{\tau}\right]^a} \exp\left[\frac{-\frac{t}{\tau}}{1 + \frac{\sqrt{1-a}}{a} \frac{t}{\tau}}\right] \quad (4)$$

with three parameters A , a and τ , which are the amplitude, the shape parameter, and the characteristic relaxation time, respectively. This function has two features: (i) an exponential decay $g_1(q, t) \sim \exp[-t/(1+(1-a)^{0.5})/\tau]$ at short times ($t \ll \tau$), and (ii) a power law decay $g_1(q, t) \sim (t\tau)^{-a}$ at long times ($t \gg \tau$). The complex decay observed here is expected not only due to an additional slow process for the stress relaxation of the heavily entangled system⁴⁴ or the gel-like system, often observed as a power law decay,⁴⁵⁻⁴⁷ but also due to the single chain dynamics on length scales of the order of the wave lengths of visible light.⁴¹ As exemplified in Figure 3, the decay at high q for the quenched DNA at 20 μ g/ml, where the DNA experiences the least inter-chain interaction, can be roughly described by the classical model for internal dynamics of a single chain, the so-called Rouse-Zimm model.⁴¹ On the other hand, the decay at low q for the unquenched DNA at 140 μ g/ml, where strong entanglement effects are expected, is found to exhibit a broad relaxation with a power law decay having a small a (≈ 0.2), similar to those of other gel-like materials,⁴⁵⁻⁴⁷ while the

decay at high q and low c yields a narrow relaxation which results in a large a ($= 0.75 \pm 0.25$).

The obtained initial relaxation rates, $\Gamma = [1+(1-a)^{0.5}]/\tau$, are found to be within errors equal to results from conventional initial slope analyses,^{41,42} and the empirical function, which covers the complete time range and includes only three parameters, results in higher stability in the fitting procedure. Figure 4 shows the q dependence of the reduced relaxation rates, $\Gamma_{\text{red}} = \eta_0 \Gamma / (k_B T q^3)$, for the quenched and unquenched DNA solutions. Here, η_0 is the viscosity of pure water, k_B Boltzmann's constant, and T the absolute temperature. We find no appreciable q dependence for the quenched solution (A) whereas clear q dependence is found for the unquenched solutions (B and C). According to de Gennes' theory of polymer solutions,^{41,48,49} the q dependence of Γ_{red} provides fundamental information of dynamics. If we consider entangled DNA solutions at $c < c^*$ at short times, the classical hydrodynamic interaction of a single chain, the so-called Zimm dynamics, is expected on length scales smaller than the mesh size of the entangled network since the segment of the DNA can be regarded as an isolated chain within the mesh. In the corresponding q range, Γ_{red} is thus predicted to have a constant value, i.e., $\Gamma_{\text{red}} \sim q^0$. (Note that Γ_{red} , by definition, has q^0 dependence when Γ has q^3 dependence.) On larger length scales, collective diffusion is anticipated at short times since the DNA then experiences random interaction with other chains. Therefore, at small q values, Γ_{red} is expected to be observed to be inversely proportional to q , i.e., $\Gamma_{\text{red}} \sim q^{-1}$, provided that the reciprocal of the mesh radius is larger than the smallest q value in the present study. On the other hand, in unentangled DNA solutions at $c < c^*$, Zimm-like behavior is expected up to the length scale of the hydrodynamic radius, $R_h \approx 0.3 \mu\text{m}$, of a single λ -DNA molecule, since the network is absent. Here the hydrodynamic radius was obtained using the theoretical relation⁴⁴ $R_h \approx 0.6 R_g$ for linear chains in a good solvent and $R_g \approx 0.5 \mu\text{m}$.¹¹ Γ_{red} is thus anticipated to be constant, i.e., $\Gamma_{\text{red}} \sim q^0$, over the whole investigated q range since the reciprocal of R_h is equivalent to the smallest q value in this study. Subsequently, the observed $\Gamma_{\text{red}} \sim q^0$ for the quenched DNA solution at $20 \mu\text{g/ml}$ (see Figure 4A) indicates that the quenched DNA is unentangled, in accordance with the structural information from AFM and AGE, although the data are scattered due to the low DNA concentration.

On the other hand, the observed clear q dependence of Γ_{red} for the unquenched DNA in solution at $20 \mu\text{g/ml}$ and $140 \mu\text{g/ml}$ (see Figure 4B and C) indicates not only the presence of the entanglement but also the mesh radius of the entangled network on smaller length scales than R_g , in good agreement with AFM results. This is shown in curve-fits using two theoretical power laws for entangled DNA solutions at $c < c^*$ (see Figure 4), giving a good description with similar parameters for both unquenched solutions. According to arguments by de Gennes,^{41,48,49} collective dynamics at short times in entangled DNA solutions with the mesh size smaller than R_h is not substantially affected by inter-chain interaction even at $c > c^*$, in sharp contrast to the behavior of conventional polymer solutions. Collective dynamics dramatically changes at even higher concentrations, where the collective dynamics is strongly affected by the presence of other DNA segments between entanglement points. From the crossover wave vector between the observed two regimes (see Figure 4B and C), the entanglement radius, ξ_E , is roughly $0.15 \mu\text{m}$ where ξ_E was obtained through $\xi_E = 1/q_0$.³⁶ The dynamical transition is therefore expected slightly above $140 \mu\text{g/ml}$, since the average inter-chain distance reaches $2\xi_E$ roughly at $200 \mu\text{g/ml}$.²⁹

Dynamic transitions in supercooled hydrated λ -phage DNA

Figure 5 presents the behavior of λ -phage DNA at the hydration level of 41.6% (gm water/gm DNA) when the temperature was increased from 123 K to 368 K. As is seen in the figure, there are three different transitions occurring within this temperature range. The one which occurred at the lowest temperature at ~ 187 K is interpreted as a dynamic transition

T_{dt} , of the biopolymers, as proposed by Rasmussen et. al.⁵⁰ At low temperatures (below 170 K, which is the onset of glass transition in Figure 5) a fraction of the bound water, especially in the first hydration shell, of DNA exists in the glassy state.^{51,52} The largest number of hydrogen bonds between the polar atoms of the oligonucleotide duplex and the surrounding water molecules is present at these low temperatures, forming a glassy layer around the DNA helix. However, at about 170 K (see the endothermic process in Figure 5) this hydration water undergoes a glass transition, due to the ‘melting’ of these hydrogen bonds of bound water molecules on the surface of the DNA.^{51,52} This ‘melting’ gives rise to a change in the overall global helicity of the DNA duplex, which is, in this case, the well defined dynamic transition⁵⁰ of the DNA duplex (shown as the exothermic peak at about 187 K in Figure 5). Thus the glass transition of the hydration water is coupled with the dynamic transition of the DNA. When we did a similar study using dehydrated DNA, this behavior could not be observed which agrees well with the idea that the dynamic transition is suppressed in dry biopolymers.⁵³ The normal outer ice region on the backbone of the DNA melts at 246 K, as shown in Figure 5. This temperature can be characterized as a crossover temperature (T_c) for the water molecules in the second and above layer of hydration around the duplex, as suggested by Sokolov et al.⁵¹ These interactions of the solvent water molecules with the DNA duplex was examined by the nature of the interaction between the polar atoms of the oligonucleotide duplex and the water molecules. This can be done by taking the ratio of T_c and T_{dt} and $T_c/T_{dt} = 1.31$, which suggests the prevalence of ionic interactions in the microenvironment as is described by Sokolov, A. P.⁵⁴ These behaviors clearly demonstrate that the dynamics of the biomolecule DNA is dictated by the motion of its surrounding water molecules at all temperatures. At the higher temperature of 355 K (T_m), the thermal melting (breaking of the H-bonds between the base pairs) of the λ -phage duplex DNA takes place (as presented in Figure 5) and the DNA denatures to form single stranded DNA.

Sequence and structural analysis of λ -Phage DNA

Structural dynamics of DNA is highly sequence dependent and the gross structural properties and large structural transitions are encoded into the physical properties of its sequence. We mapped the variation of nucleotide distribution on the λ -phage genome by analyzing the cumulative GC profile to understand the structure-function correlation of the genome. The GC profile of phage genome shows an interesting feature as shown in Figure 6.

The overall GC content of λ -phage genome is high. The initial 21.5 kb region of the phage DNA is very GC rich with 56.9% GC content and the remaining sequence has an average GC content of 44.2%. The GC content varies in different organisms and is a signature of selection processes during evolution. The cumulative GC profile reveals that in the initial 21.5 kb sequence there is a continuous rise in GC content. At 21.5 kb (the square on the curve in Figure 6) there is an abrupt drop in the cumulative GC profile, indicating that there is a clear boundary between the genomic islands. This point of the negative cumulative GC profile, called segmentation point, is a clear indication of genomic boundary that may result due to the horizontal gene transfer signifying functional relevance and signature of evolution. Throughout the phage genome there is only one segmentation point according to the GC profile. This point divides the phage genome into two distinct regions of different physical properties. It is known that DNA with high GC-content is more stable than DNA with low GC-content. We have analyzed various physical and structural parameters of initial 29 kb genomic sequence of phage genome due to limited computational resources. Our main focus was to analyze the effect of segmentation on the physical properties of phage DNA, and therefore we include an additional 7.5 kb genomic sequence of phage DNA after the segmentation point at 21.5 kb, such that we can visualize both sides of the segmentation point on the basis of physical parameters. Figures 1S (A and B) show the plot of duplex

disruption and stabilization free energies versus number of bases where it is clear that the section before the segmentation point is more stable compared to the rest of the genome.

Bendability and curvature analysis of λ -phage DNA

The variation of DNA bendability and its associated parameters along the λ -phage genome is depicted in Figure 7. Due to the biphasic distribution in the GC content of the phage genome, it possesses also a biphasic pattern of DNA bendability. The absolute value of the bendability correlates positively with the GC content; whereas the curvature correlates negatively as is mentioned by Vinogradov⁵⁵ and supported by Figure 2S. The calculation of DNA bendability of phage genome reveals that it possesses an overall symmetric bendability distribution. Thus, the phage genome is expected to be rigid in solution. In this context it is important to mention that the sequences before the segmentation point, i.e. in the high GC content region has a more symmetric distribution of DNA bending propensity, while for the remaining of the phage genome, an anisotropic bending distribution was observed.

Figures 7B and C display that two parameters, the stacking energy and the propeller twist, are highly correlated with the bendability of DNA. The GC rich region has an average base pair stacking energy of -9 to -9.5 kcal/mol. It is known that on a dinucleotide physical scale the GC pair has the highest stacking energy of -14.6 kcal/mol, while the AT pair has the lowest stacking energy of -3.82 kcal/mol.⁵⁶ The presence of G and C enhances the base stacking energy. A clear biphasic sequence profile of phage DNA also significantly affects the two parameters; stacking energy distribution and propeller twist profile. The GC rich section has an average melting temperature of $82-85$ °C while the AT rich region possess an average melting temperature of $74-77$ °C according to Figure 7D. This is in agreement with our experimentally observed melting temperature of λ -phage DNA of 82 °C in Figure 5.

Low frequency normal mode dynamics of λ -phage DNA at the segmentation point and upon entanglement

The 21623th sequence of phage DNA is the segmentation point. We have simulated 30 base pairs from both sides of the segmentation point using an elastic network model considering the cohesive ends in entangled form. Large scale dynamics of long stretches of DNA sequences has been successfully modeled as a worm-like chain. So, we applied a simplified elastic network model to capture the dynamics of the DNA around the segmentation point. Deformations have been generated along the low frequency vibration modes using the duplex DNA. First three orthogonal Cartesian translations and rotations of the molecule as a whole around the principal axis of its inertia tensor of the molecule are not considered. It has been observed that the calculated low frequency modes of DNA are collectively associated with large scale changes in the three dimensional structure. The five lowest frequency modes depict the symmetric vibration of the duplex DNA along its helical axis. Thus, a symmetric bending was observed by simulating the DNA around the segmentation point in its lowest frequency vibration mode (Figure 8). It is pertinent to mention that when DNAs are entangled, the AT rich section from one phage DNA align with a GC rich section of another phage DNA to join. In this way a segmentation point is added, which allows a symmetric bending pattern of λ -phage DNA.

Energetics, structure and chromatin dynamics of free and entangled λ -phage DNA

λ -phage DNA has free sticky ends that readily hybridize to form entangled DNA. We have calculated the enthalpy of formation of entangled phage DNA in different forms and the results are summarized in Table 1.

It is evident from the table that the entangled DNA most probably adopts B-DNA conformation, which is energetically most favorable, while the entangled region has the least probability to adopt A-DNA conformation. Critical insight into the entangled DNA structural parameters reveal that the average value of rise increases to 3.67 Å (compared to 3.3 Å in B-DNA) and twist angle decreases to 31.57° (compared to 36° in B-DNA),⁵⁷ thereby making the entangled DNA's appearance to be stretched. The duplex entangled DNA appears to be little longer in the major groove and compressed minor groove than the standard B-form of DNA. Base pairs in the entangled form have the usual Watson-Crick hydrogen bonding pattern, but the free end bases are more flexible, as shown in Figure 9A.

The free cohesive end of the λ -phage DNA also appears to be little stretched, specially the 3'-end, where the backbone is deformed making the stacking of the bases difficult. So in Figure 9A, the last two bases at 3'-end are tilted away from the helical axis. Thus, it is evident from the structural and energetic parameters that free cohesive ends are more flexible and bendable, and hybridization in a B-form reduces the deformation as the ends are packed by hydrogen bonding interactions. To further study the effect of entanglement on the bendability pattern of the λ -phage DNA, we studied chromatin dynamics of the free and entangled phage DNA using DNALive web interfaces and the results are displayed in Figure 9. DNALive produces a rapid representation of chromatin dynamics, which showed a surprisingly high accuracy of the essential deformation pattern of DNA. As evident from Figure 9A right, the dynamics is highly distributed in a spherical manner in unentangled DNA. Thus all possible bending and curvatures can be observed in the chromatin dynamics distribution. On the other hand, as is presented in Figure 9 B right, when the DNA is entangled, the DNA bending stiffness increases and comparatively linear chromatin dynamics distribution is observed around the midpoint of the DNA fragments, which is basically the segmentation point in this case. This gives rise to the symmetric bending distribution around the segmentation point in entangled DNA which supports observations from Figure 8.

CONCLUSION AND SUMMARY

We have investigated the structure and dynamics of entangled and hydrated chromosome-sized DNA using experimental and theoretical perspectives. The present study demonstrates the following: When long DNA molecules are formed by hybridization of the cohesive ends of λ -phage DNA at high concentrations, the resulting macromolecules show signatures of a heavily entangled network in both structure and dynamics, even after the dilution of the same DNA solutions below the overlap concentration c^* of the λ -phage monomer. Such a structural memory indicates that the disentanglement upon dilution is very slow, at least on the time scale of several weeks. This observation is indicative of the entangled DNA-polymers of sizes at least up to the λ -phage decamer, corresponding to contour lengths of several hundred micrometers. The global transition of the 41.6% hydrated λ -phage DNA is coupled to the dynamics of the surrounding water molecules, as evident from the ratio of the crossover temperature and the dynamic transition temperature, where a value of 1.31 indicates the presence of strong ionic interactions between DNA and its microenvironment. Sequence analysis reveals a biphasic cumulative GC content distribution in phage DNA, which dictates structural and functional properties of λ -phage genome. Theoretical modeling and molecular mechanics calculations reveal that the entangled region most likely adopts a B-DNA conformation and upon entanglement a symmetric bending distribution has been observed in this region. The results obtained in our study constitute the fundamental elements for grammar recognition, by which a DNA duplex talks to protein. These important elements open new perspectives to a better understanding of the effect of different parameters on DNA mechanical properties and a way to modulate it, empowering the

existing knowledge of DNA-protein interactions involved in genome regulation and packaging.

Supplementary Material

Refer to Web version on PubMed Central for supplementary material.

Acknowledgments

We acknowledge financial support from the Swedish Research Council and Magn. Bergwall Foundation. We like to acknowledge Professor Bjorn Akerman and Niklas Boseus of Department of Chemical and Biological Engineering, Chalmers University of Technology for allowing us performing gel electrophoresis experiment in his laboratory and in the interpretation of the result. BSG likes to thank the research support from NIH/ NCMHHD/RIMI grant # 1P20MD002725 at Tougaloo College. BSG also thanks Professor Pradeep K. Sengupta of SINP, India for giving access to HYPERCHEM software of his lab, which is used in this study.

REFERENCES AND NOTES

1. Bloomfield, VA.; Crothers, DM.; Tinoco, I. Nucleic acids. Structure, Properties and Functions. University Science Books; Sausalito: 2000. p. 13-41.
2. Hur JS, Shaqfeh ESG, Babcock HP, Smith DE, Chu S. J. Rheol. 2001; 45:421–450.
3. Hård T, Kearns DR. Biopolymers. 1986; 25:1519–1529. [PubMed: 3742003]
4. Livolant F, Leforestier A. Prog. Polym. Sci. 1996; 6:1115–1164.
5. Seol Y, Li J, Nelson PC, Perkins TT, Betterton MD. Biophys. J. 2007; 93:4360–4373. [PubMed: 17766363]
6. Dickerson RE. Nucleic Acid Res. 1998; 26:1906–1926. [PubMed: 9518483]
7. Bertin A, Mangenot S, Renouard M, Durand D, Livolant F. Biophys. J. 2007; 93:3652–3663. [PubMed: 17693471]
8. Perkins TT, Smith DE, Chu S. Science. 1994; 264:819–822. [PubMed: 8171335]
9. Robertson RM, Smith DE. Proc. Natl. Acad. Sci. USA. 2007; 104:4824–4827. [PubMed: 17360350]
10. Lysetskaya M, Knoll A, Boehringer D, Hey T, Krauss G, Krausch G. Nucleic Acid Res. 2002; 30:2686–2691. [PubMed: 12060686]
11. Verma R, Crocker JC, Lubensky TC, Yodh AG. Phys. Rev. Lett. 1998; 81:4004–4007.
12. Becker A, Gold M. Proc. Natl. Acad. Sci. USA. 1978; 75:4199–4203. [PubMed: 279909]
13. Vinograd J, Lebowitz JJ. Gen. Physiol. 1966; 49:103–125.
14. Fried MG, Bloomfield VA. Biopolymers. 1984; 23:2141–2155. [PubMed: 6498295]
15. Wang JC, Davidson NJ. Mol. Biol. 1966; 19:469–482.
16. Jary D, Lal J, Sikorav JLCR. Acad. Sci. III. 1998; 321:1–4.
17. Wang JC, Davidson N. J. Mol. Biol. 1966; 15:111–123. [PubMed: 5912035]
18. Dawson JR, Harpst JA. Biopolymers. 1971; 10:2499–2508. [PubMed: 5126521]
19. Hershey AD, Burgi E. Proc. Natl. Acad. Sci. USA. 1965; 53:325–328. [PubMed: 14294064]
20. Rockland LB. Anal. Chem. 1960; 32:1375–1376.
21. Kumar P, Yan Z, Xu L, Mazza MG, Buldyrev SV, Chen S-H, Sastry S, Stanley HE. Phys. Rev. Lett. 2006; 97:177802–177806. [PubMed: 17155508]
22. Hormeño S, Moreno-Herrero F, Ibarra B, Carrascosa JL, Valpuesta JM, Arias-Gonzalez JR. Biophys. J. 2011; 100:2006–2015. [PubMed: 21504737]
23. Tao NJ, Lindsay SM, Rupprecht A. Biopolymers. 1988; 27:1655–1671. [PubMed: 3233323]
24. Saminathan M, Thomas T, Shirahata A, Pillai CKS, Thomas TJ. Nucleic Acid Res. 2002; 30:3722–3731. [PubMed: 12202757]
25. Castellano C, Generosi J, Congiu A, Cantelli R. Appl. Phys. Lett. 2006; 89:233905, I–III.
26. Symons MCR. Cell. Mol. Life Sci. 2000; 57:999–1007. [PubMed: 10961340]
27. Bednarek J, Plonka A, Hallbrucker A, Mayer E, Symons MCR. J. Am. Chem. Soc. 1996; 118:9387–9390.

28. Mamontov E, O'Neill H, Zhang Q. *J. Biol. Phys.* 2010; 36:291–297. [PubMed: 21629590]
29. Lyubchenko YL, Shlyakhtenko LS. *Proc. Natl. Acad. Sci. USA.* 1997; 94:496–501. And References Therein. [PubMed: 9012812]
30. Liu Z, Li Z, Zhou H, Wei G, Song Y, Wang L. *Microsc. Res. Techniq.* 2005; 66:179–185.
31. Liu Z, Li Z, Zhou H, Wei G, Song Y, Wang L. *J. Microscopy.* 2005; 218:233–239.
32. Waterbury PG, Lane MJ. *Nucleic Acids Res.* 1987; 15:3930. [PubMed: 2954030]
33. Birren BW, Lai E, Clark SM, Hood L, Simon MI. *Nucleic Acids Res.* 1988; 16:7563–7582. [PubMed: 3412895]
34. Gao F, Zhang CT. *Nucleic Acids Res.* 2006; 34(Web Server issue):W686–W691. [PubMed: 16845098]
35. Goñi JR, Fenollosa C, Pérez A, Torrents D, Orozco M. *Bioinformatics.* 2008; 24:1731–1732. [PubMed: 18544548]
36. Vlahovicek K, Kajan L, Pongor S. *Nucleic Acids Res.* 2003; 31:3686–3687. [PubMed: 12824394]
37. Bolshoy A, McNamara P, Harrington RE, Trifonov EN. *Proc. Natl. Acad. Sci. USA.* 1991; 88:2312–2316. [PubMed: 2006170]
38. Suhre K, Sanejouand YH. *Nucleic Acids Res.* 2004; 32:W610–W614. [PubMed: 15215461]
39. Dogett NA, Smith CL, Cantor CR. *Nucleic Acids Res.* 1992; 20:859–864. [PubMed: 1542577]
40. Åkerman B, Cole KD. *Electrophoresis.* 2002; 23:2549–2561. [PubMed: 12210158]
41. Schaefer, DW.; Han, CC. *Dynamic Light Scattering: Applications of Photo Correlation Spectroscopy.* Pecora, R., editor. Plenum Press; New York, New York: 1985. p. 181–243.
42. Bloomfield, VA. *Dynamic Light Scattering: Applications of Photo Correlation Spectroscopy.* Pecora, R., editor. Plenum Press; New York, New York: 1985. p. 363–416.
43. Svanberg C. *J. Appl. Phys.* 2003; 94:4191–4197.
44. Wang CH. *Prog. Colloid Polym. Sci.* 1993; 91:138–141.
45. Shukla A, Fuchs R, Rehage HJ. *Langmuir.* 2006; 22:3000–3006. [PubMed: 16548549]
46. Nyström B, Kjøniksen AL. *Langmuir.* 1997; 13:4520–4526.
47. Ren SZ, Shi WF, Zhang WB, Sorensen CM. *Phys. Rev. A.* 1992; 45:2416–2422. [PubMed: 9907263]
48. deGennes, PG. *Scaling Concepts in Polymer Physics.* Cornell University Press; Ithaca, New York: 1979. p. 69–97.
49. Teraoka, I. *Polymer solutions: An Introduction to Physical Properties.* Wiley-Interscience; New York: 2002.
50. Rasmussen B,F, Stock AM, Ringe D, Petsko GA. *Nature.* 1992; 357:423–424. [PubMed: 1463484]
51. Sokolov AP, Grimm H, Kahn R. *J. Chem. Phys.* 1999; 110:7053–7057.
52. Anagnostopoulou A, Daoukaki D, Pissis P, Loukakis G, Sideris EG. *J. Non-Crystalline Solids.* 1991; 131-133:1182–1185.
53. Ferrand M, Dianoux AJ, Petry W, Zaccai G. *Proc. Natl. Acad. Sci. USA.* 1993; 90:9668–9672. [PubMed: 8415760]
54. Sokolov AP. *Science.* 1996; 273:1675–1676.
55. Vinogradov AE. *Nucleic Acids Res.* 2003; 31:1838–1844. [PubMed: 12654999]
56. Hesselmann A, Jansen G, Schütz M. *J. Am. Chem. Soc.* 2006; 128:11730–11731. [PubMed: 16953592]
57. Cooper VR, Thonhauser T, Puzder A, Schroder E, Lundqvist BI, Langreth DC. *J. Am. Chem. Soc.* 2008; 130:1304–1308. [PubMed: 18163624]
58. Zheng G, Lu X-J, Olson WK. *Nucleic Acids Res.* 2009; 37:W240–W246. [PubMed: 19474339]

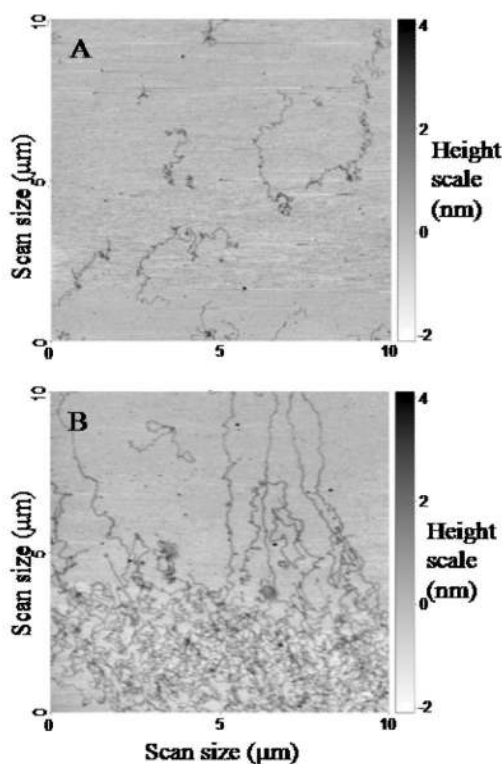


Figure 1.

Typical AFM height images of structures for quenched (A) and unquenched (B) λ -DNA molecules at 0.1 $\mu\text{g/ml}$ in solution after immobilization onto APTES-modified muscovite mica sheets. Images were second-order plane-fitted using the Scanning Probe Image Processor (SPIP; Image Metrology Inc., Denmark). The scan size was 10 μm , and the height scale is 6 nm for both images.

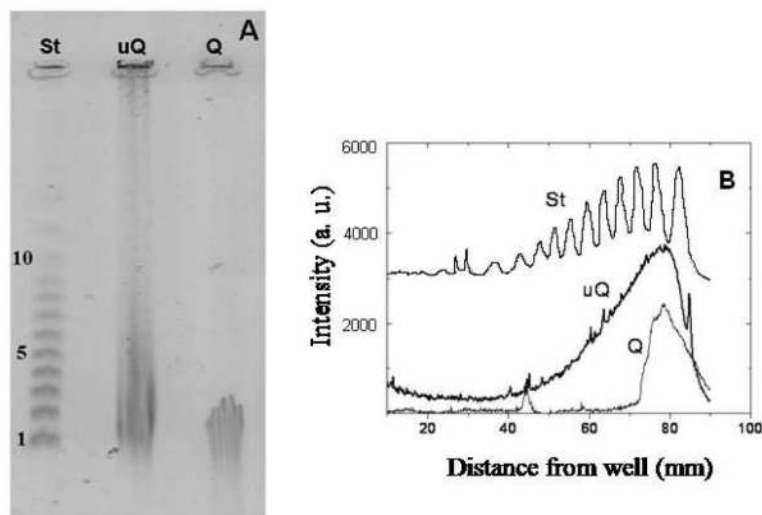


Figure 2.

Analysis of the agarose gel electrophoresis pattern of hybridized λ -phage DNA. The unquenched sample (uQ) was hybridized for 7 days at 20 °C (see text for details), the quenched sample (Q) was heated for 65 °C for 10 minutes before loading on the gel. The total DNA concentration was 150 $\mu\text{g/ml}$ in both cases. (A) Gel image was taken after ethidium bromide staining. The λ -ladder molecular weight standard (St) contains the oligomers indicated by the numbers on the left. (B) Intensity profiles along the full width of the lanes in (A). Electrophoresis conditions: 1% agarose, 120° pulse angle, $T_p = 30$ s, 6 V/cm, 17 °C, 16 hours running time.

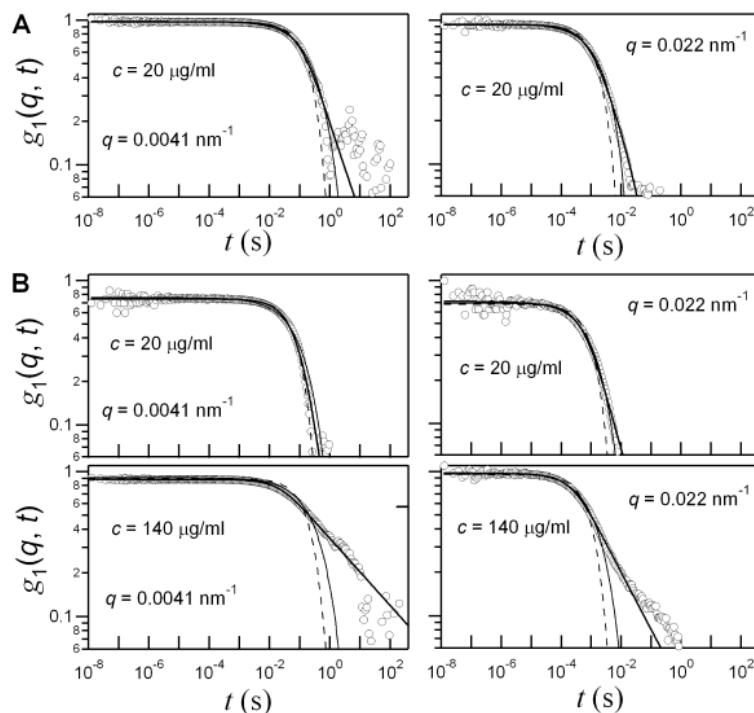


Figure 3.

PCS data of typical field correlation functions, $g_1(q, t)$, at 25 °C for quenched (A) and unquenched (B) λ -phage DNA solutions. Left column is for $q = 0.0041 \text{ nm}^{-1}$ and right column is for $q = 0.022 \text{ nm}^{-1}$. The concentrations are $20 \mu\text{g/ml}$ for the quenched DNA solution (A), and $20 \mu\text{g/ml}$ (top) and $140 \mu\text{g/ml}$ (bottom) for the unquenched DNA solutions (B). Here, q is scattering wave vector, and t time. The thick solid lines represent curve-fits using Equation 4. The thin solid lines represent curve fits using the Rouse-Zimm model with $\exp[-(t/\tau_0)^{2/3}]$, where τ_0 is the relaxation time,³² while the dashed lines represent curve-fits using a pure exponential decay.

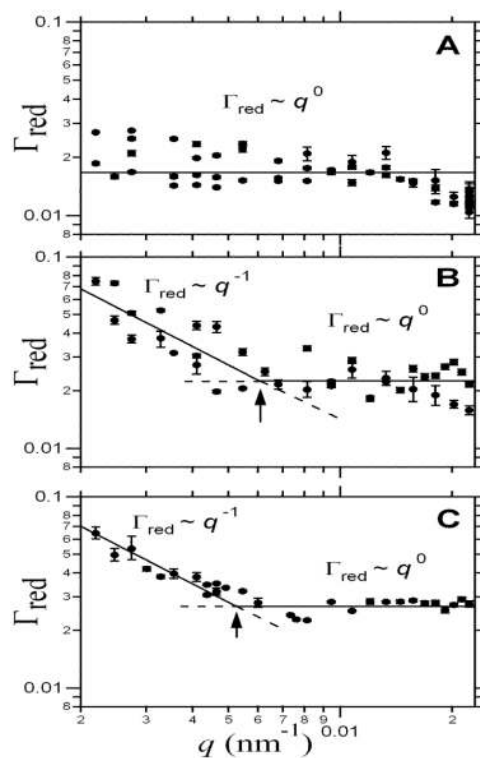


Figure 4.

The scattering wave vector, q , dependence of the reduced relaxation rates, Γ_{red} , at 25 °C for quenched (A) and unquenched (B) λ -DNA in solution at 20 $\mu\text{g/ml}$, and the unquenched DNA solutions at 140 $\mu\text{g/ml}$ (C). The solid lines represent curve fits using $\Gamma_{\text{red}} = \Gamma_{\text{red}0} q_0 q^{-1}$ ($q < q_0$) and $\Gamma_{\text{red}} = \Gamma_{\text{red}0}$ ($q \geq q_0$), where q_0 is the crossover wave vector indicated by the arrows. The dashed lines are extrapolations of the power laws into the neighboring regime. For the quenched DNA solution in panel A, we do not observe any appreciable crossover and $\Gamma_{\text{red}0}$ is 0.017 ± 0.001 . For the unquenched DNA solutions in panels B and C, $\Gamma_{\text{red}0} = 0.023 \pm 0.001$, $q_0 = 0.0060 \pm 0.0005 \text{ nm}^{-1}$ (20 $\mu\text{g/ml}$) and $\Gamma_{\text{red}0} = 0.026 \pm 0.001$, $q_0 = 0.0053 \pm 0.0002 \text{ nm}^{-1}$ (140 $\mu\text{g/ml}$).

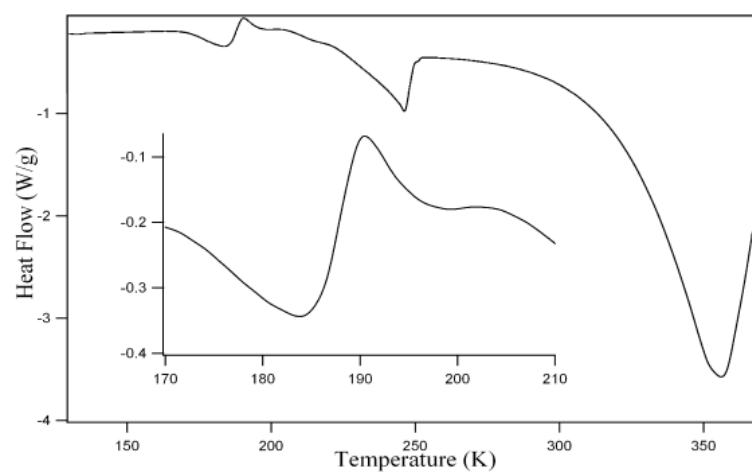


Figure 5.

Study of the dynamic transition ($T_{dt} = 187$ K), the crossover temperature ($T_c = 246$ K) and the thermal unfolding leading to denaturation ($T_m = 355$ K) of 41.6% hydrated (w water/w DNA) λ -phage DNA by differential scanning calorimetry. The cooling/heating rates were 10 K/min. Inset: The temperature range around the dynamic transition is highlighted.

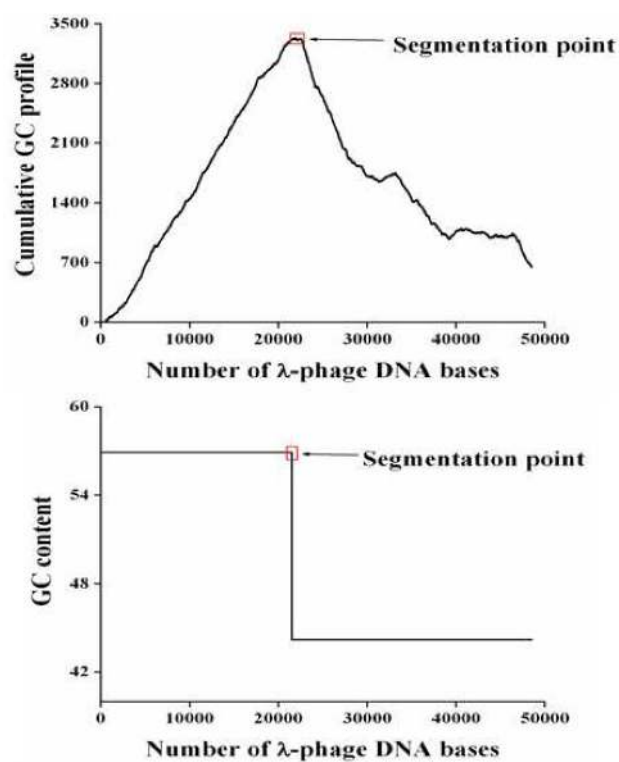


Figure 6. Cumulative GC profile of λ -phage genome. The square shows the segmentation point on the λ -phage genome.

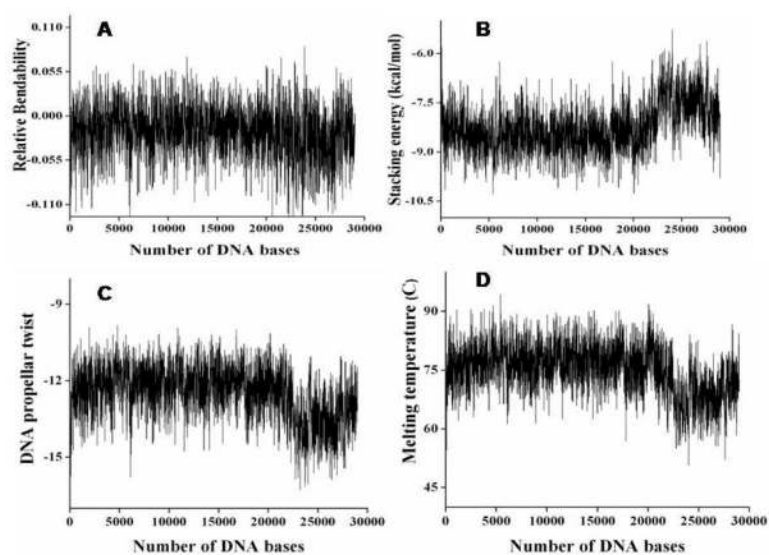


Figure 7. Variation of bendability (A) and its associated parameters e.g. base pair stacking (B), DNA propeller twist (C), and melting temperature (D) along the 29 kb λ -phage genome.

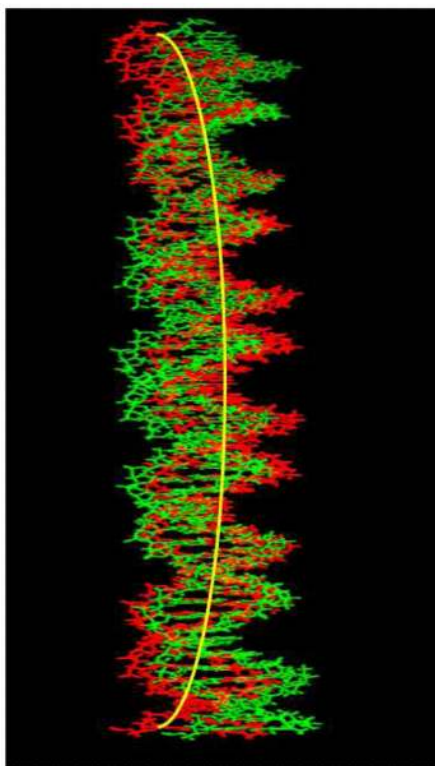


Figure 8. Deformation of λ -phage DNA around the segmentation point (60 base pair), simulated in its lowest frequency normal mode using an elastic network model. Bending axis is shown in yellow.

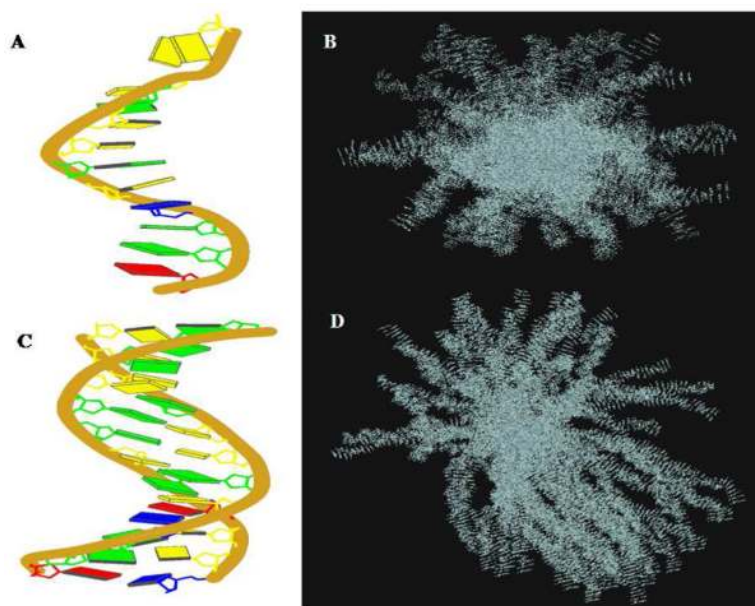
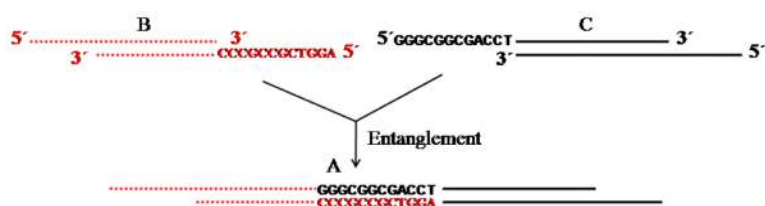


Figure 9.

Left (A and C): Structures of cohesive end which are generated using the 3DNA web-server.⁵⁸ Right (B and D): Chromatin dynamics of λ -phage DNA which are performed using DNALive web-server. A and B represent unentangled while C and D display entangled forms respectively.

**Scheme 1.**

A: Typical diagram of an entangled λ -phage DNA. Different forms of lines represent various λ -phage DNA molecules in the entangled state. B and C: λ -phage DNA with 5'-cohesive ends.

Table 1
Calculated energy and enthalpy of formation of free and entangled λ -phage DNA in different forms

DNA name ^r	Form	Energy (kcal/mol)	Formation enthalpy (kcal/mol)
3'-sticky ends		-590.29	
5'-sticky ends		-567.16	
Entangled DNA	A	-1077.39	80.06
	B	-1331.57	-174.12
	Z	-1156.31	1.15

^rPlease refer to Scheme 1 for structures.